THE JOURNAL OF PHYSICAL CHEMISTRY C

ARTICLE

pubs.acs.org/JPCC

Experimental (XAS, STEM, TPR, and XPS) and Theoretical (DFT) Characterization of Supported Rhenium Catalysts

Simon R. Bare,*[,†] Shelly D. Kelly,[§] Fernando D.Vila,[∥] Edwin Boldingh,[†] E. Karapetrova,[‡] Josh Kas,[∥] George E. Mickelson,[†] Frank S. Modica,[†] Ning Yang,[‡,⊥] and John J. Rehr[∥]

[†]UOP LLC, A Honeywell Company, Des Plaines, Illinois 60016, United States

[‡]Argonne National Laboratory, Argonne, Illinois 60439, United States

[§]EXAFS Analysis, Bolingbrook, Illinois 60440, United States

[∥]Department of Physics, University of Washington, Seattle, Washington 98195, United States

Supporting Information

ABSTRACT: A high surface area supported Re-based catalyst, fundamental to heterogeneous catalysis, is studied in the oxidic and reduced states using a combination of experimental (XAFS, STEM, TPR, and XPS) and theoretical (DFT and X-ray spectroscopy simulations) approaches. In the calcined dried catalyst, the Re species is present as an isolated trioxo(oxoaluminate) Re(VII) species. The temperature at which the Re undergoes reduction is a function of the hydrogen partial pressure and temperature ramp rate, but the maximum rate of reduction occurs in the range 300−400 °C. Following reduction at 500 or 700 °C in dry hydrogen, the Re is present as a mixture of species: unreduced trioxo(oxoaluminate) Re(VII) species, Re nanoclusters, and isolated Re atoms. By using a multifaceted approach, it is apparent that the majority species is an isolated Re adatom bound to the alumina support. DFT calculations identify several likely adsorption sites for these Re adatoms on the [110] surface of γ-Al_2O_3. The final extended X-ray absorption fine structure (EXAFS) model taking into account these three species is used to identify the dominant adsorption site for Re on the alumina surface. FEFF8 X-ray absorption near-edge spectroscopy (XANES) calculations of unsupported and alumina-supported Re nanoclusters provide interpretation of the shape and edge position of the Re L_3-edge XANES after reduction. The presence of moisture during reduction strongly affects the mobility of the Re on the alumina leading to agglomeration. Subsequent air exposure of a reduced catalyst readily reoxidizes the reduced Re. The power of using a combination of analysis tools provides insight into the behavior of dispersed Re on supported alumina under oxidizing and reducing conditions relevant to heterogeneous catalysis.

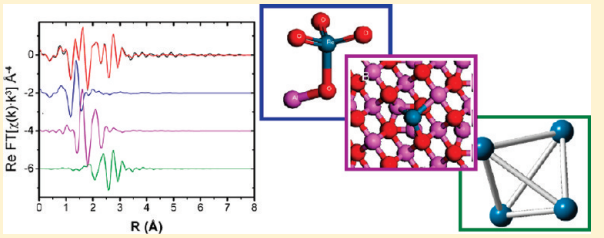

INTRODUCTION

Supported rhenium catalysts are of great technological importance in heterogeneous catalysis. In the oxidic form, rhenium oxide dispersed on high surface area alumina has been shown to have high activity and high selectivity in olefin metathesis.[1] Supported Re catalysts also show high activity for selective catalytic oxidation of simple alcohols[2,3] and exhibit activity in hydrodesulfurization and hydrodenitrogenation.[4] When rhenium forms a bimetallic cluster with platinum, the subsequent Pt−Re clusters are used in petroleum-reforming catalysts.[5,6] Given this ubiquitous nature of rhenium-based catalysts, it is not surprising that they have been the focus of several characterization efforts which are briefly summarized below. Rhenium is a particularly interesting metal as it is strongly oxophilic and its chemistry is therefore expected to be dominated by its propensity for forming strong metal−oxygen bonds, quite different from the more traditionally studied group VIII metal-based catalysts.

In reviewing the prior characterization work, it is clear that the nature of the supported rhenium species for catalysts prepared by standard methods using, for example, incipient wetness impregnation of soluble rhenium compounds is complex and warrants further detailed studies under controlled conditions. For example, the reducibility of oxidic rhenium on alumina has been a topic of discussion for decades, and the issue has still not been fully resolved. Going back to the 1970s there are numerous papers discussing the reducibility of rhenium on alumina.[7−9] The debate centered on how much of the rhenium is reduced. This debate continued into the 1980s[10,11] with similar discrepancies as to the temperature of maximum reduction and the amount of reduction. In the current decade the issue of the reducibility of rhenium continues to be a topic of discussion.[12] From these and other studies it can be concluded that the rhenium loading, calcination temperature, and effect of adsorbed moisture all play a role in determining the reducibility of rhenium.

XAFS has previously been used to probe the structure of supported rhenium catalysts. Ellison et al.[13] concluded that after

Received: November 3, 2010
Revised: January 19, 2011
Published: March 08, 2011

dx.doi.org/10.1021/jp1105218 | J. Phys. Chem. C 2011, 115, 5740–5755

calcination of a 15 wt % Re (as the oxide)/γ-alumina catalyst extended X-ray absorption fine structure (EXAFS) spectra could be modeled with a single shell of four oxygen atoms at 1.73 Å. Their data did not support the presence of any Re−Re interaction. For the sample with less than 10 wt %, a better fit to their data was achieved when they split the first oxygen shell into two O atoms at 1.71 Å and two at 1.74 Å. They suggested that these data were consistent with the rhenium being present as a "Re_2O_7"-like species. Hardcastle et al.[14] used Re L_1-edge (X-ray absorption near-edge spectroscopy) XANES data to conclude that the structure of the rhenium oxide complex on the alumina surface is the same from 0.1 to 12 wt % Re and resembles that of the structure of the Re in ammonium perrhenate. Hence, the local coordination of the rhenium species is tetrahedral with four Re−O bonds.

Fung et al.[15] reported EXAFS data following in situ reduction at 450 °C of a 1.0 wt % Re/γ-Al_2O_3 sample. They fit their data with two Re−O contributions, 2O at 2.07 Å and 1.5O at 2.60 Å, and a Re−Re shell with a coordination number of 4.5 at 2.74 Å. They concluded that the short Re−O at 2.07 Å suggested that a fraction of the Re species remained oxidized after the 450 °C reduction. An interesting observation in this work was that even after the 450 °C reduction the intensity of the white line at the L_3-edge is still comparable to that of rhenium(IV) oxide, ReO_2, where the rhenium is in the formal oxidation state +4. The authors stated that this observation indicates that the Re in the reduced catalyst has an average oxidation state of +4. They reconcile this statement by suggesting that the sample consisted of a mixture of reduced and oxidized Re species after the reduction treatment.

Rønning et al.[16] concluded that, for 2 wt % Re in the oxidized form, the EXAFS data could be modeled using a single Re−O coordination shell, with coordination number and interatomic distance equivalent to that of $[ReO_4]^-$, i.e., four oxygen atoms at a distance of 1.74 Å . After a 6 h reduction at 450 °C, they modeled the EXAFS data with two Re−O shells and two Re−Re shells. The Re−O contributions arise from unreduced rhenium oxide and from the alumina support oxygen. The first Re−Re shell at 2.74 Å has a coordination number of 5, and the second shell has a coordination number of 3.0 at 3.65 Å. The authors conclude that the data are consistent with about 80% of the rhenium being reduced into 15 Å diameter clusters, with the remaining present as a rhenium oxide.

A recent paper by Lobo-Lapidus and Gates[17] reported the use of EXAFS to characterize several rhenium-containing complexes and clusters on γ-Al_2O_3. The clusters were prepared from $H_3Re_3(CO)_{12}$ and the catalysts tested in the hydrogenolysis of *n*-butane. In all cases they conclude that the Re is cationic, and the Re−Re first-shell coordination number of approximately two, is consistent with trirhenium clusters bonded to the support.

A brief summary of the X-ray absorption fine structure (XAFS) characterization of 0.7 wt % Re on the 75% MOR/25% Al_2O_3 following reduction in moist hydrogen at 500 °C has previously been published.[18] This study showed that dispersed, but agglomerated, Re nanoparticles (~30 Å diameter) are primarily formed, with a predominant sheet-like shape rather than spherical or cuboctahedral particles. It was proposed that these oblate-shaped clusters were formed as a result of the strong interaction of the Re with the alumina surface.

In addition to these XAFS studies, there have been studies using other characterization techniques; a few of the relevant studies are discussed and summarized here. A series of papers (using primarily chemisorption methods, XPS, Raman, and electron microscopy) by Okal et al.[19−24] focused on the reduction and reoxidation behavior of Re/γ-Al_2O_3 catalysts, concluding with a review of their detailed work probing the structure and activity of these catalysts.[25] Focusing only on the wt % Re loadings relevant to this study (1 wt %) it was concluded that the Re is highly dispersed after reduction at 550 and 800 °C, and only a few clusters could be detected by HRTEM. Given the low number of observable clusters, no particle size distributions could be obtained. Even after high temperature reduction (800 °C) the Re cluster size only ranged from 10 to 40 Å, with an average of 21 Å. The XPS data were characterized by a single broad peak instead of distinct Re $4f_{7/2}$ and $4f_{5/2}$ peaks, indicating strong interaction of the Re with the support. The Raman spectra of the oxidized catalyst show only a single weak band at 1000 cm^{-1}, assigned to the terminal Re═O symmetric stretching vibration of the tetrahedral surface rhenium oxide species that is distorted by strong interaction with the alumina support. They concluded that rhenium is coordinated to the alumina support as a ReO_4 monomer. They noted that even short air exposure at room temperature of the small reduced Re clusters resulted in complete reoxidation. Okal et al. concluded that even though significant progress has been made in the understanding of the chemistry of supported rhenium oxide catalysts a detailed description of the species is still lacking and requires further study.

Supported rhenium oxide catalysts were also the focus of a Raman, FTIR, XPS, and TPR study by Mitra et al.[12] Under ambient conditions the Raman spectra showed a strong band at 977−991 cm^{-1} and a weak band at 920 cm^{-1}, independent of rhenium oxide loading, and were consistent with the presence of isolated ReO_4^- species. Under dehydrated conditions the Raman spectra changed to a single band at 1000 cm^{-1} assigned to the terminal Re═O bond. They propose that the surface Re species present is either four or five coordinated, isolated, and possesses one or more Re═O functionalities. The exact structure of the surface rhenium oxide could not be determined in this study. However, it was concluded in an earlier Raman study by the same group[14] that the supported rhenium oxide is present as an atomically dispersed surface $[ReO_4]_{ads}$ species with C_{3v} symmetry, consistent with the presence of three equivalent terminal Re−O bonds and one inequivalent Re−O bond, taken to result from the Re−O−Al bonding which anchors the species to the alumina surface.

Both Shpiro et al.[26] and Yide et al.[27] studied the form of Re on γ-Al_2O_3 supported catalysts by XPS. The conclusion from both studies is that the Re is present as +7 in the oxidized form but after hydrogen reduction there is a mixture of Re oxidation states present and that conclusive determination of the oxidation state(s) could not be reached using XPS alone.

From these observations it can be surmised that under standard catalyst preparation conditions (impregnation of aqueous oxidic rhenium species) followed by calcination and reduction the rhenium is present as a mixture of species. This complexity has contributed to the confusion and discrepancies in the details of many of the previous studies.

In this paper these complications are addressed by using a combination of theoretical and experimental methods together with modern analysis techniques. In particular a Re catalyst supported on γ-Al_2O_3 has been characterized using XAFS, STEM, TPR, and XPS and theoretical methods including density functional theory (DFT) and X-ray spectroscopy simulations using the real-space Green's function based FEFF8 code.

We elucidate detailed information about the molecular structure of the calcined oxidized form of rhenium and after reduction at 500 and 700 °C using dry hydrogen. The rate and extent of Re reduction is studied using TPR and in situ XANES. The Re L_3-edge XANES of the reduced catalyst is compared to FEFF8 XANES calculations of free and alumina-supported Re nanoclusters. DFT calculations are used to identify the most likely adsorption site for the Re adatoms on the (110) surface of γ-Al_2O_3. On the basis of the DFT calculations, EXAFS modeling is used to identify the dominant site for reduced Re adatoms. The effects of moisture on Re reduction and subsequent air exposure of a reduced catalyst are also presented.

EXPERIMENTAL SECTION

Materials Preparation. The Re-based catalyst was made by evaporative impregnation of an ammonium perrhenate solution onto a 75% MOR (Si/Al_2 = 20)/25% Al_2O_3 base. After the impregnation the catalyst was calcined in dry air at 540 °C for 2 h. The metal loading of the catalysts was determined by ICP. The majority of the work was conducted on a sample containing 0.7 wt % Re, but two others containing 0.14 and 0.4 wt % Re were prepared for the TPR measurements.

Re metal powder, rhenium(IV) oxide (ReO_2), rhenium(VI) oxide (ReO_3), and ammonium perrhenate (NH_4ReO_4) were prepared as XAFS standards. These were purchased from Aldrich and used as received. The phase purity of each was checked using powder XRD from which it was determined that no other phases were present.

Materials Characterization. *XPS.* XPS data were collected using a Physical Electronics Quantum2000 scanning ESCA microprobe using monochromatic Al K_α radiation. Elemental survey scans were collected using a pass energy of 187 eV and the individual region scans using a pass energy of 29 eV. The instrument's built-in dual charge compensation methodology using dual low-energy electrons and low-energy argon ions was used. The spectra were charge referenced to Al 2p = 74.0 eV. XPS data were collected both after drying (ramp at 5 °C/min to 500 °C in flow of 20% O_2/He, dwell for 20 min at 500 °C, cool to room temperature in O_2/He before evacuating the cell for direct transfer to the spectrometer) and after reduction at 500 °C (ramp at 4 °C/min to 500 °C in flow of 100% H_2, dwell for 30 min at 500 °C, cool to room temperature in hydrogen before evacuating the cell for direct transfer to the spectrometer). Both treatments were performed in a custom-designed reactor directly attached to the XPS instrument. This allowed transfer of the sample from the reactor to the UHV of the instrument without air exposure of the sample.

TPR. The extent of metal reduction is quantitatively measured using a custom-built apparatus with programmed temperature control. A known concentration of hydrogen (5%) in argon gas is passed over a fixed amount of sample (250 mg) in a quartz reactor, while the temperature is increased at a linear rate. Downstream of the reactor the water in the gas phase is then trapped before the effluent is sent to a thermal conductivity detector. The difference in hydrogen concentration before, during, and after reduction is measured. The apparatus is calibrated using a series of five injections through a fixed sample loop (0.2 cc) of 100% hydrogen before each experiment to obtain quantitative data on the extent of reduction of metal oxide(s) at the selected temperatures.

STEM. The STEM data of the reduced catalysts were collected on a VGHB601UX scanning transmission electron microscope operated at 100 kV. Sample transfer and preparation was performed in a nitrogen purged glovebag to minimize any exposure to the air and subsequent reoxidation of the catalyst.

XAFS. Samples for the XAFS experiments were made by hand pressing the catalyst powder into a quartz tube. The weight of the sample was calculated to have an absorption length of about 2.0 and the fractional absorbance by Re of approximately 0.2. The sample was placed in a custom-designed in situ reactor allowing for both high-temperature treatment and cooling to liquid nitrogen temperature for EXAFS measurements. Full details of the equipment are presented elsewhere.[28] The gas flow was controlled using an automated gas manifold. The catalyst samples were reduced in situ during XAS measurements using the following methods. The sample was loaded into the reactor and then dried by incremental heating at 5 °C/min in a flow of 20% oxygen/80% helium to 525 °C followed by a dwell at 525 °C for 30 min followed by cooling to room temperature. This sample is referred to as "oxidized". EXAFS data were then collected on the resulting oxidized dried sample at room temperature. The sample was then reduced in flowing hydrogen (99.999% purity, 60 sccm, purified by passing through a MatSen purifier) by incremental heating at 4 °C/min to 500 °C followed by a dwell of 30 min at 500 °C. Re L_3-edge XANES scans were collected during the incremental heating. After dwelling at 500 °C for 30 min, the sample was cooled to room temperature in the flow of hydrogen and then to a final temperature of −180 °C (using liquid nitrogen as coolant) in a flow of helium. Multiple EXAFS scans were collected at liquid nitrogen temperature to improve the averaged signal-to-noise ratio. This sample is referred to as "dry reduced 500". The reduction experiment was duplicated using a fresh sample of catalyst but using a maximum reduction temperature of 700 °C. This sample is referred to as "dry reduced 700". A third experiment was conducted to investigate the effect of moisture during the reduction. In this experiment the catalyst was not dried in situ and was reduced in a flow of hydrogen flowing through a distilled water saturator held at 25 °C. This gives a moisture content of the hydrogen of 3.1 mol %. The sample was reduced by heating at 4 °C/min to 500 °C. This sample is referred to as the "wet reduced 500".

The X-ray absorption spectra were measured at the X18B beamline of the National Synchrotron Light Source (NSLS) at Brookhaven National Laboratory and at beamline 33BM at the Advanced Photon Source at Argonne National Laboratory. At the NSLS the energy of the electron in the storage ring is 2.5GeV with a ring current of 150−160 mA. The Si(111) monochromator was detuned 30% to minimize the content of the higher harmonics incident on the sample. A white beam slit of 1 mm was used to improve energy resolution. The APS storage ring was operated at 7 GeV with a constant ring current of 105 mA. A double crystal monochromator with Si(111) crystals was used to select the incident X-ray energy. The X-rays of higher harmonic energies were removed by two Rh-coated mirrors, with the first mirror also acting as a collimator and the second as a focusing mirror. All the measurements were performed in transmission at the Re L_3 edge, and the EXAFS scans were collected to 18 $Å^{-1}$. The energy was calibrated by setting the maximum of the first derivative of the Re L_3 absorption edge of the Re powder sample to 10535.0 eV. During the measurement of the catalyst the Re powder reference was placed between the transmission (I_t) and reference (I_{ref}) ion chambers to allow absolute energy calibration for each XAFS scan.

XAFS spectra of the reference samples were collected in transmission using finely ground powders dispersed on tape, with the appropriate thickness to give approximately two total absorption lengths.

Theoretical Modeling Methods. DFT calculations were carried out in an effort to identify the most likely adsorption site for the Re adatoms on the [110] surface of γ-Al_2O_3. The DFT optimizations used the PBE exchange-correlation functional,[29] a plane-wave cutoff energy of 396 eV, and standard ultrasoft pseudopotentials.[30] They were carried out on the "d" layer of the [110] surface of γ-Al_2O_3 using VASP.[31] The simulations used a 13.68 Å × 9.68 Å surface cell that provides a variety of interaction sites such as O and Al atoms and a vacancy. The simulation cell included four layers of atoms separated by 20 Å of vacuum. The starting point of the Re atom interaction relaxations was produced by first mapping the interaction energy of a Re atom located 2.2 Å above the surface. The points associated with the largest interaction energies were then used to initiate the optimizations. This approach yielded five distinct minima. All calculations were performed using the DOE NERSC and UW high-performance computer facilities.

Theoretical XANES Methods. Real space multiple scattering calculations of the XANES together with the angular momentum projected density of states (LDOS) were carried out using a parallel version of the FEFF8.4 code.[32] This approach has been found to be well-suited for heavy metals XAS studies.[33] These full-multiple-scattering (FMS) calculations use muffin-tin potentials generated self-consistently, a fully screened core-hole, and the default Hedin−Lundqvist[34] plasmon-pole self-energy. All calculations used an angular momentum cutoff of l_{max} = 3 for scattering from the Re atoms, l_{max} = 2 for scattering from Al atoms, and l_{max} = 1 for scattering from O atoms. In cases where nonequivalent Re atoms were present, configurational averaging was carried out to obtain the XANES spectrum.

EXAFS Modeling Methods. EXAFS data reduction and analysis were performed using Athena,[35] which is an interface to IFEFFIT,[36] and FEFFIT.[37] The data were modeled in R-space with theoretical models constructed from FEFF.[38] The models were simultaneously refined to the EXAFS data processed with a *k*-weight of 1, 2, and 3 in the Fourier transforms. The data ranges ($Å^{-1}$), fit ranges (Å), independent points in the EXAFS spectrum,[39] and the number of variables determined in the models for all the EXAFS spectra are given in the Supporting Information, Table SV.

The EXAFS models are parametrized in terms of the local atomic environment of the absorbing atom. All atoms of the same type with the same average distance from the absorbing atom have the same contribution to the EXAFS signal; hence, the EXAFS models are based on the contributions from shells of atoms about the absorber. Each shell is described by a path that originates at the absorbing atom (Re), goes to one or more neighboring atoms, and then returns to the absorbing atom. These paths are denoted by Re−Re*X* for the *X* shell of Re atoms. For example, the Re−Re1 path in bulk Re metal is the single scattering path from the absorbing Re atom to the 6 nearest-neighbor Re atoms, all at the same distance (2.74 Å) from the absorbing atom. The number of atoms in a shell is the degeneracy (N_{degen}), and the average distance between the absorbing atom and the neighboring atoms is given by the bond length (R). Since all atoms within a shell are not at exactly the same distance from the absorbing atom, a relative mean-square displacement of the atom pairs of the path (σ^2) is also used in the models. The σ^2-term includes contributions from both thermal and static disorder. The final two parameters in the EXAFS models are an energy shift (ΔE_0) and the passive electron reduction factor S_0^2. The EXAFS signal can be modeled by trial and error with a few dominant scattering paths. Each of these paths will have at least three parameters (N_{degen}, R, and σ^2) such that the information content within the data is quickly reached. We call this type of modeling "molecular moiety modeling" because a general average molecular environment of the Re atoms can be deduced. Another approach is to base the EXAFS model on a DFT calculation for Re on the alumina surface. This approach uses many more paths but with fewer variables. For example, only *x*, *y*, and *z* coordinates for Re (three variables) are used to determine the *R* values for all paths. From this type of modeling we can determine if the data are consistent with a proposed detailed structure. These models are compared by using the reduced-χ^2 value that takes into account the differences in the number of variables used in the different models.

Using theoretical standards from FEFF to model EXAFS spectra requires an estimate of the passive electron amplitude reduction factor S_0^2. This parameter depends mostly on the excited atom type, so it is often determined by modeling known materials containing the absorbing element of interest. To a lesser extent, S_0^2 may also be influenced by the experimental setup and sample preparation.[40] This variation is usually well within the experimental accuracy of the EXAFS measurement. To demonstrate the independence of S_0^2 with respect to the sample, EXAFS data from two rhenium-containing standards of known crystallographic structure were collected: rhenium metal and ammonium perrhenate. Because of its physical properties, Re foil of the appropriate thickness for EXAFS measurements at the Re L_3-edge (approx 5 μm thick) can not be commercially obtained. A proper powder sample for transmission EXAFS measurements has a particle size that is significantly less than one absorption length such that a uniform sample can be prepared by either spreading the particles on tape or dispersing them within a binder such as boron nitride (or other light Z) powder. The metallic rhenium sample used for transmission EXAFS measurements was prepared from a Re metal powder of −325 mesh, so containing metal particles <44 μm. This is many absorption lengths in thickness (1 absorption length above the Re L_3 edge is 2.2 μm). Therefore, total electron yield spectra were also collected from a freshly cleaned and abraded thick rhenium foil. Electron yield measurements are typically more difficult due to the smaller cross section of Auger electrons produced at the surface that predominantly give the electron yield signal, but this method has the advantage that it is not affected by the thickness of the sample.

Insight is gained regarding the degree of transferability of the S_0^2 parameter by modeling Re standards from compounds with different valence states. The experimental data, modeling results, and discussion are supplied in the Supporting Information (Supplemental Figures S1−S3 and Supplemental Tables SI−SIV).

RESULTS

1. Determination of Average Rhenium Oxidation State Using XANES. The Re L_3-edge XANES can be used to determine average Re oxidation state of supported rhenium catalysts. The intensity of the white line and the absorption edge energy position are both indicators of the average rhenium oxidation state. XANES spectra of reference oxidic compounds with Re in different formal oxidation states were measured: rhenium metal,

Re(0); rhenium(IV) oxide, ReO_2; and ammonium perrhenate, Re(VII) $(NH_4)ReO_4$. The XANES spectra of these materials are plotted in the Supporting Information, Figure S4. There is a significant shift in the absorption edge with formal oxidation state of the rhenium in addition to an increase in the white line intensity. The inset of Figure S4 (Supporting Information) shows a plot of the energy of the maximum of the first derivative of the absorption edge versus formal rhenium oxidation state.[41] There is an approximately linear shift in absorption edge position with increasing oxidation state.[15] Using this empirical correlation the average rhenium oxidation state of the oxidic rhenium in an unknown sample can be estimated.

The XANES data of the reference compounds were measured in both transmission mode and in total electron yield. With the exception of the spectra for rhenium metal, the transmission data and total electron yield data are similar. For metallic rhenium there is evidence for a thickness effect in the spectrum measured in transmission from the rhenium powder compared to that from the Re foil in electron yield as the white line intensity is attenuated (Supporting Information, Figure S4). However, analysis of EXAFS data from both data sets is nearly identical as shown in the Supporting Information, Figure S1. These data highlight the care that must be taken when using white line intensity as a fingerprint of the presence of metallic rhenium.

2. Oxidized Catalyst. In a typical preparation of a supported metal catalyst the material is prepared by impregnation using an appropriate aqueous solution of the metal followed by calcination in air to decompose the precursors and to leave the active metal dispersed on the support in an oxidic form. This is the procedure used for the preparation of the rhenium catalysts in this study. A full understanding of the metal−support chemistry and subsequent evolution of the active form of the catalyst (following reduction) can only be achieved by studying each of the preparation steps. In this section the results of the characterization of the oxidized catalyst are presented.

The Re 4f XPS spectrum of the oxidized catalyst after drying at 500 °C is shown in the Supporting Information, Figure S5. The spectrum can be fit to a spin−orbit split doublet with the Re $4f_{7/2}$ at 46.0 eV binding energy and a full width at half-maximum of 2.8 eV. This indicates that the formal Re oxidation state is +7 in the dried oxidized catalyst.[26,27]

The Re L_3-edge XANES spectra of the as-received catalyst and after in situ drying are compared in the Supporting Information, Figure S6. There is a subtle change in the Re L_3-edge XANES between the as-received catalyst and that after in situ drying. The form of the rhenium in the as-received catalyst is not studied further as the degree of hydration was not controlled and is likely influenced by the amount of adsorbed moisture. The focus instead is on the dried oxidized catalyst. The absorption edge position of the dried catalyst is the same as for the ammonium perrhenate standard indicating that the formal oxidation state of the rhenium in the dried oxidized catalyst is primarily Re(VII), in agreement with the XPS data.

The EXAFS data of the dried oxidized catalyst are plotted in Figure 1. Figure 1A shows a plot of the $\chi(k)\cdot k^2$ data which shows good signal-to-noise ratio to 15 $Å^{-1}$. The distance of the first peak in the magnitude of the Fourier transformed spectrum (Figure 1B) is consistent with neighboring oxygen atoms. Several models were considered for this data set, including a single Re−O path, split Re−O paths for the signal between 1 and 2 Å in the FT, and longer Re−Al or Re−Re paths for the signal between 2 and 3 Å. The model with a split Re−O path and a Re−Al path was statistically better than any of the other models. The reduced χ^2 was at least a factor of 10 less for this model compared to all others considered.

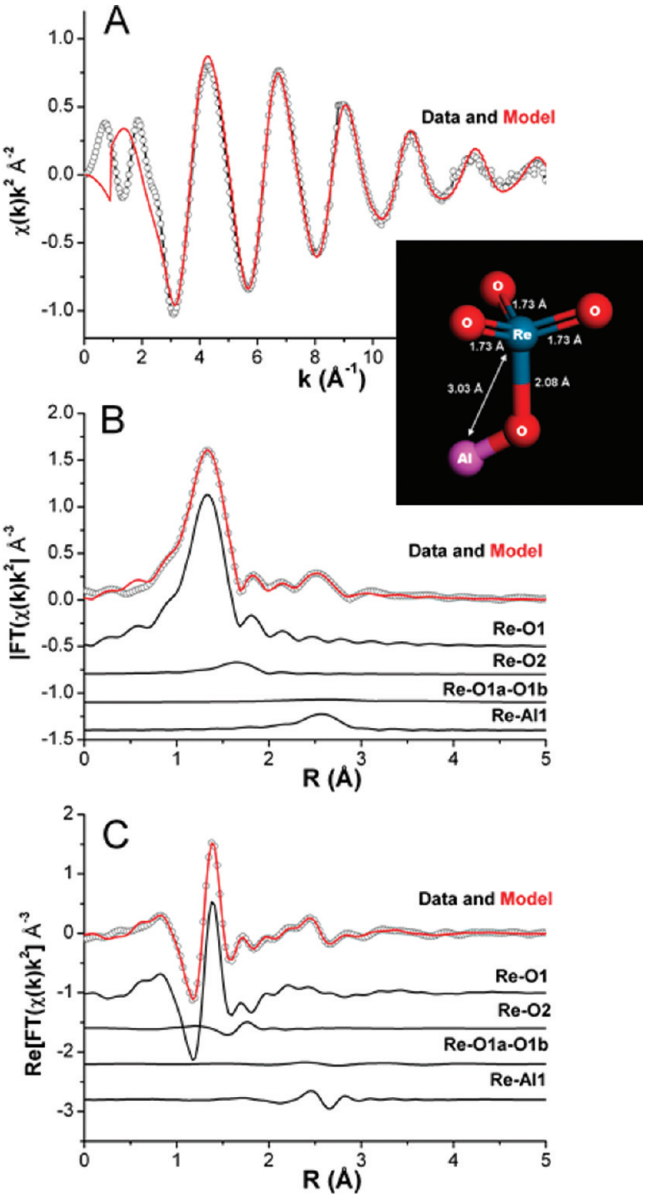

Figure 1. Re EXAFS data from oxidic Re (symbols) and model (line). (A) EXAFS $\chi(k)\cdot k^2$ data. (B and C) Magnitude and real part of Fourier transform. The components of the model are shown offset beneath the measured spectra and model. The inset shows a schematic of the oxidized Re species on the alumina.

Table I. Best Fit of the Oxidic Re in the Sample[a]

path description	N_{degen}	R (Å)	σ^2 ($\cdot 10^{-3}$ Å^2)
Re0−O1	3.5 ± 0.1	1.73 ± 0.01	3 ± 2
Re0−O2	0.5 ± 0.1	2.08 ± 0.01	3 ± 2
Re0−O1a−O1b	3.5 ± 0.1	3.45 ± 0.01	12 ± 8
Re0−Al1	1.0 ± 0.1	3.03 ± 0.01	3 ± 2

[a] The spectrum was modeled with two oxygen paths and one aluminum path. The N_{degen} of the first two oxygen paths was constrained so that the sum was 4, and their σ^2 values were set to be the same. The ΔR was determined for each single scattering path.

dx.doi.org/10.1021/jp1105218 |J. Phys. Chem. C 2011, 115, 5740–5755

Table II. Theoretical Amount of Hydrogen Needed for Reduction of the Rhenium Together with the Actual Hydrogen Consumption Determined by Integrating the Area under the Hydrogen Uptake Peak in the TPR

oxidation state change	theoretical yield (mmol/g)	actual consumption 500 °C reduction (mmol H_2/g)	amount of reduction 500 °C	actual consumption 700 °C reduction (mmol H_2/g)	amount of reduction 700 °C
Re(VII) to (0)	0.117	0.080	68.5%	0.098	84%

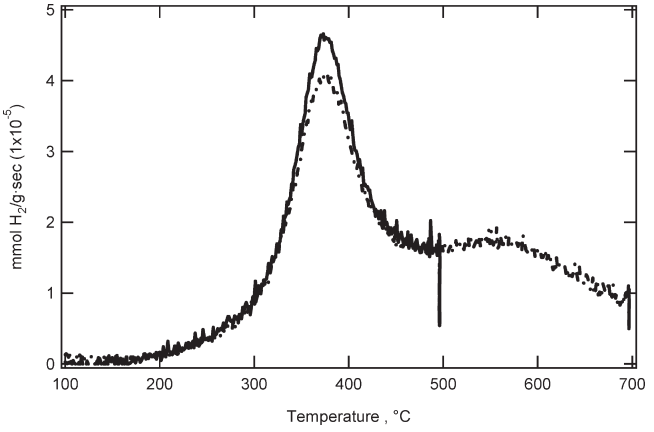

Figure 2. Temperature-programmed reduction of the catalyst. Ramp at 4 °C/min to 500 °C and held 30 min (solid) and to 700 °C and held 30 min (dashed).

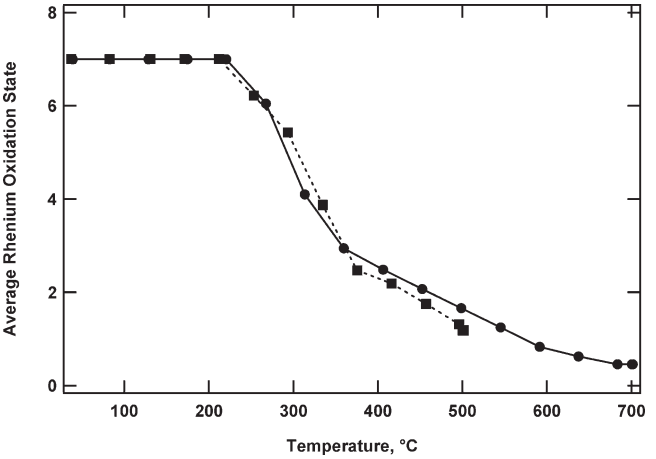

Figure 3. Average rhenium oxidation state as a function of temperature calculated from the XANES spectra shown in the Supporting Information, Figure S5. Reduction up to 500 °C (squares) and 700 °C (circles).

The best fit parameters are listed in Table I. The spectrum was modeled with two Re−O signals and one Re−Al signal. There are 3.5 ± 0.1 oxygen atoms at 1.73 ± 0.01 Å, 0.5 ± 0.1 oxygen atoms at 2.08 ± 0.01 Å, and 1.0 ± 0.1 aluminum atoms at 3.03 ± 0.01 Å. These results are consistent with rhenium in the oxidized catalyst surrounded by four oxygen ligands in a distorted tetrahedral arrangement (three short and one longer Re−O bond). The longer O signal and the Al signal are presumed to be from the surface of the alumina as depicted in the structural model shown as an inset in Figure 1. This model is in good agreement with other studies on the structure of dispersed rhenium oxide at low loadings on alumina.[14]

3. Dry Hydrogen Reduction. The active form of a dispersed supported metal catalyst is typically obtained after reduction, where the oxidic precursors are reduced in a flow of hydrogen resulting in the highly dispersed metallic nanoclusters. Two samples were thus characterized following dry hydrogen reduction, one after a medium temperature reduction to 500 °C and the second after a higher temperature reduction to 700 °C. In both cases the reduced samples were generated by heating in a flow of 100% H_2 at a ramp rate of 4 °C/min and held at the maximum reduction temperature for 30 min.

Standard temperature programmed reduction data are shown in Figure 2. This figure shows an overlay of the rate of hydrogen uptake versus temperature for the 500 and 700 °C maximum temperature reduction experiments. There is a reduction peak at 375 °C and a second, broader peak centered at 550 °C. The total hydrogen uptake determined by integrating the area under the peak is summarized in Table II. These TPR data imply that there is incomplete reduction of the rhenium, even after heating to 700 °C for 30 min. If the assumption is made that the reduction is from Re(VII) to Re(0) then 84% of the Re is reduced (16% remains as Re(VII)) after the 700 °C reduction, and only 68.5% is reduced after the 500 °C reduction (31.5% remains oxidic). Figure S7 (Supporting Information) shows the TPR of catalysts prepared from 0.14, 0.4, and 0.7 wt % Re. At the low Re loading (<0.4 wt %), the low temperature reduction peak is absent.

The Re 4f XPS spectrum of the 500 °C reduced catalyst is shown in the Supporting Information, Figure S5. The spectrum appears as a single broad peak centered at ~43.6 eV binding energy with no well-defined separation of the spin−orbit splitting. It was not possible to obtain a unique satisfactory fit to this spectrum using well-defined binding energies and reasonable full-widths at half maxima of the peaks. However, it is clear that the centroid of the peak moves to lower binding energy as compared to the oxidized spectrum indicating that there is reduction of the Re. The broadness and overall shape of the 4f region suggest that there is likely a distribution of Re oxidation states present. This observation is in agreement with prior XPS studies of other supported rhenium catalysts.[26,27]

Figures S8A and S8B (Supporting Information) show the evolution of the Re L_3-edge XANES as the oxidized, dried catalyst is heated in a flow of 100% hydrogen from room temperature to 500 °C (A) and 700 °C (B) at a rate of 4 °C/min. The white line intensity decreases, and there is a shift in the edge position to lower energy with increasing temperature. Both of these observations indicate that the rhenium undergoes reduction. Using the previously determined linear relationship between the formal rhenium oxidation state and the absorption edge position (Supporting Information, Figure S4), the resulting average rhenium oxidation state as a function of temperature is shown in Figure 3. At the end of the 500 °C reduction the average oxidation state of the rhenium is 1.2, and after the 700 °C reduction the average oxidation state is 0.5. There is good agreement between the two data sets over the temperature range where they overlap. The average oxidation states determined from the edge position are lower than those calculated using the hydrogen uptake measurements in the TPR which correspond to 2.2 after 500 °C reduction and 1.1

dx.doi.org/10.1021/jp1105218 |J. Phys. Chem. C 2011, 115, 5740–5755

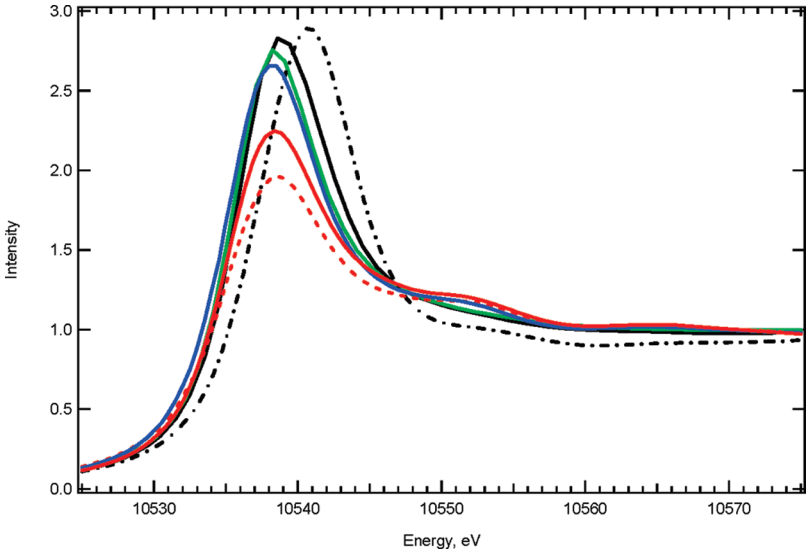

Figure 4. Comparison of the Re L_3-edge XANES of the 500 °C (black) and 700 °C (green) reduced catalyst samples with those of Re foil in TEY (red), Re metal powder (red, dashed), and ReO_2 (black, dot-dash). Also shown is the spectrum after the wet reduction (solid blue).

after 700 °C reduction but we believe are in reasonable agreement given the approximations involved.

Figure 4 shows a comparison of the Re L_3-edge XANES spectra of the catalyst after the 30 min hold at 500 and 700 °C with the XANES of Re metal (powder and TEY of Re foil) and ReO_2. The white line intensity of the 700 °C reduced sample is slightly lower than that of the 500 °C reduced sample. The edge position after reduction is similar to that of metallic rhenium, but the intensity of the white line is similar to that of Re(IV) oxide. The implication is that the rhenium in the reduced catalyst is present primarily in a cationic state. A similar conclusion was reached by Fung et al.[15] and Lobo et al.[17] A simple linear combination fit of the XANES of Re metal and Re(VII) oxide does not account for the data—even though the TPR suggests the presence of both of these species, as does the EXAFS modeling (see below). For comparison the XANES spectrum following the wet hydrogen reduction (see below) is also shown. The white line intensity is smaller than that of the dry reduced catalysts, but still more intense than that of the bulk rhenium metal. Also note the intensity of the resonance at ~10 553 eV. This feature is essentially absent in the 500 and 700 °C reduced samples but is clearly observed in the XANES of the wet reduced sample and bulk Re metal.

To provide some understanding of the experimental observations, theoretical XANES calculations were performed to probe both the effect of rhenium cluster size and the interaction of the rhenium clusters with the alumina surface on the Re L_3-edge XANES. Re L_3 XANES and local density of states (LDOS) of Re clusters of varying size were calculated with and without the effect of the alumina substrate. All of the Re clusters were cut directly from the bulk crystal. Clusters of 3, 4, 13, 19, and 57 atoms were used to represent nanoparticles, while a cluster of 93 atoms was used to simulate bulk rhenium metal. The results of the calculation for these clusters are shown in Figure 5. There is a reduction in white line intensity and shift to higher photon energy with increasing cluster size, with the most substantial changes occurring from 3- to 13-atom Re clusters. The figure also shows an enlargement of the resonance at ~10 553 eV. The intensity of this resonance scales approximately with the Re cluster size. These same-sized rhenium clusters were then attached to the alumina substrate by assuming that the triangular face of the cluster would bond to a triangular face of the (110)-terminated alumina surface formed by three surface oxygen sites and FEFF XANES calculation performed of the surface bound clusters. The Re−O bond lengths were taken to be ~2.07 Å. Figure 6 shows schematically the 3- and 13-atom clusters bound to the alumina support. The results of these L_3-edge XANES calculations are shown in Figure 7. The white line intensity and edge position are now similar for both the 3- and 13-atom clusters. These calculated XANES spectra are then compared with the experimental XANES spectra in Figure 8. There is good agreement between the calculated bulk Re spectrum (93 atoms) and the experimental metallic Re spectrum. The white line intensity of the 700 °C reduced catalyst is, however, larger than that from the calculation of the small clusters on the alumina surface. The corresponding LDOS calculations of the free and supported 3- and 13-atom Re clusters are shown in the Supporting Information, Figure S9. From these calculations we see that including the support causes a shift of amplitude from below to above the Fermi level in both clusters. This is associated with electron transfer from the Re clusters to the support. Charge counts were calculated for all of the Re atoms in both the 3- and 13-atom clusters. Both clusters are positively charged, with the average charge per atom being 0.243 for Re_3 and 0.190 for Re_{13}. In addition, for the Re_{13} cluster, the Re atoms near the surface are more cationic than those in the second and third layer, with the Re at the center of the cluster (second layer) being almost neutral.

STEM data of the 500 and 700 °C dry reduced samples are shown in Figure 9. After 500 °C reduction the rhenium cluster size ranges from 5 to 8 Å, with an average of ~7 Å, and after 700 °C reduction the cluster size is a little larger, with a range of 5−15 Å with an average of ~8 Å. It is noted that it was difficult to find a substantial number of Re clusters in the microscope. Thus, it is believed that many of the Re clusters are so small that they are not observable in the STEM images.

The detailed modeling of the Re L_3-edge EXAFS data of the catalysts (below) was performed on catalysts that were subsequently cooled to −173 °C after in situ reduction. During the cooling there is the possibility of partial reoxidation of the

dx.doi.org/10.1021/jp1105218 |J. Phys. Chem. C 2011, 115, 5740–5755

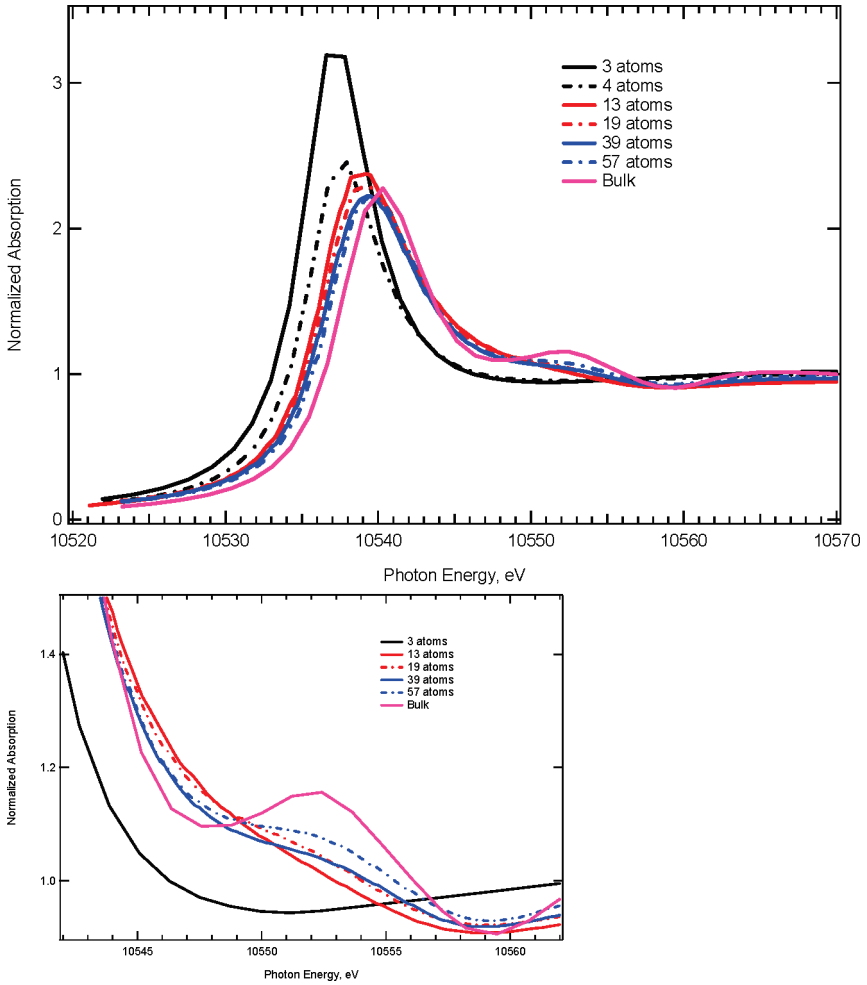

Figure 5. Theoretical Re L_3-edge XANES of naked Re clusters of various sizes. The overall XANES spectra (top) and enlargement of the feature at 10 552 eV (bottom). The feature at 10 552 eV grows as a function of cluster size.

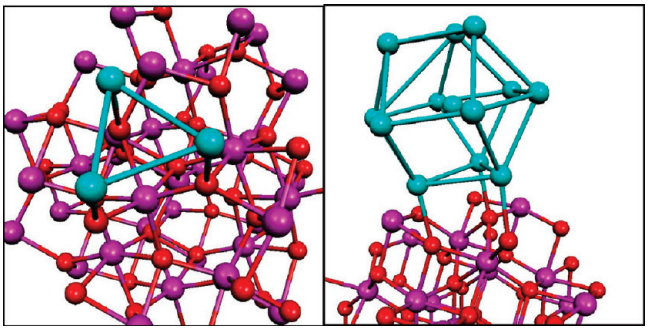

Figure 6. Structure of Re clusters of 3 (left) and 13 (right) atoms on alumina support. These structures were used for the calculations of XANES and LDOS.

catalyst. The XANES spectra of the catalyst recorded at 500 °C and at 700 °C are compared to their respective spectra at liquid nitrogen temperature in the Supporting Information, Figure S10. The spectra recorded at elevated temperature and those acquired at liquid nitrogen temperature are identical, indicating that there is no measurable reoxidation of the rhenium during the cooling.

A comparison of the Re L_3-edge EXAFS spectra from the 500 and 700 °C dry reduced samples is shown in Figure 10. Overall, the spectrum from the 500 °C dry reduced sample is similar to that from the 700 °C sample. The EXAFS signal, shown in Figure 10A, has maxima at approximately 4.5, 7.5, 8.9, and 11.5 $Å^{-1}$ and minima at approximately 5, 7, 8.5, 11, and 12 $Å^{-1}$. There is a shift in the peak at 6 $Å^{-1}$ in the 500 °C reduction data to 6.5 $Å^{-1}$ in the 700 °C reduction spectrum. In addition, the EXAFS oscillations of the 500 °C reduction spectrum are larger than those of the 700 °C reduction spectrum. The magnitude and real part of the FT are shown in Figure 10B and Figure 10C, respectively. The differences in the spectra are dominated by the region between 1 and 2 Å, where the magnitude of the FT of the 500 °C reduction spectrum is larger than the 700 °C spectrum.

Initially the dry reduced spectra were modeled using a molecular moiety. In this modeling approach each of the dominant signals is accounted for with a scattering path, as previously discussed for the dried oxidic Re sample. The EXAFS signal was mostly accounted for by including a Re−O1 path, a Re−O2 path, a Re−Al path, and a Re−Re path. The modeling results are listed in Table III. The Fourier transform of the EXAFS spectra and the contribution from each path to the model are shown in Figure 11. This figure illustrates the interference between the Re−O1 and Re−O2 signals used in the model. It is believed that the interference of these two scattering paths results in the very small measured EXAFS signal in these samples. The model also shows that some Re−Re signal is also required to account for the data. This implies that there is at least some Re cluster formation

dx.doi.org/10.1021/jp1105218 |J. Phys. Chem. C 2011, 115, 5740–5755

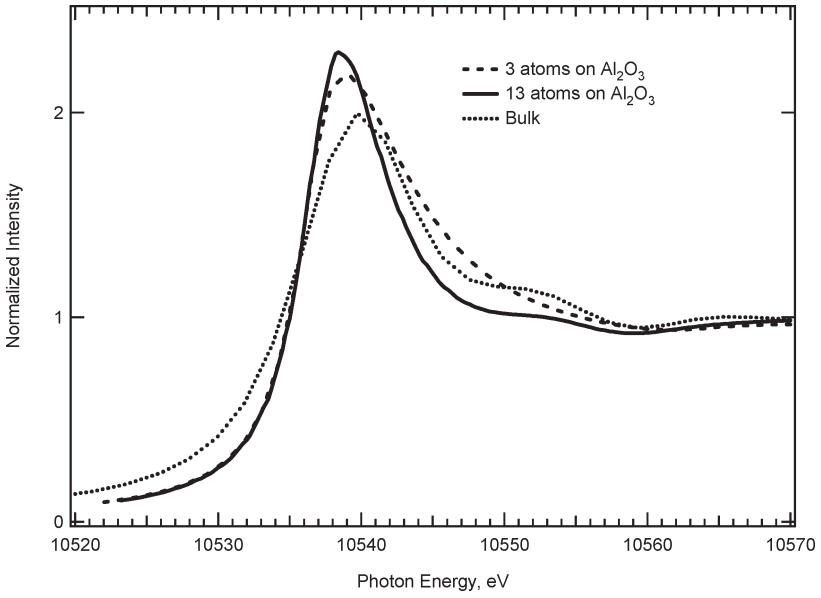

Figure 7. Theoretical Re L_3-edge XANES of the 3- and 13-atom Re clusters interacting with an alumina surface together with that of the bulk.

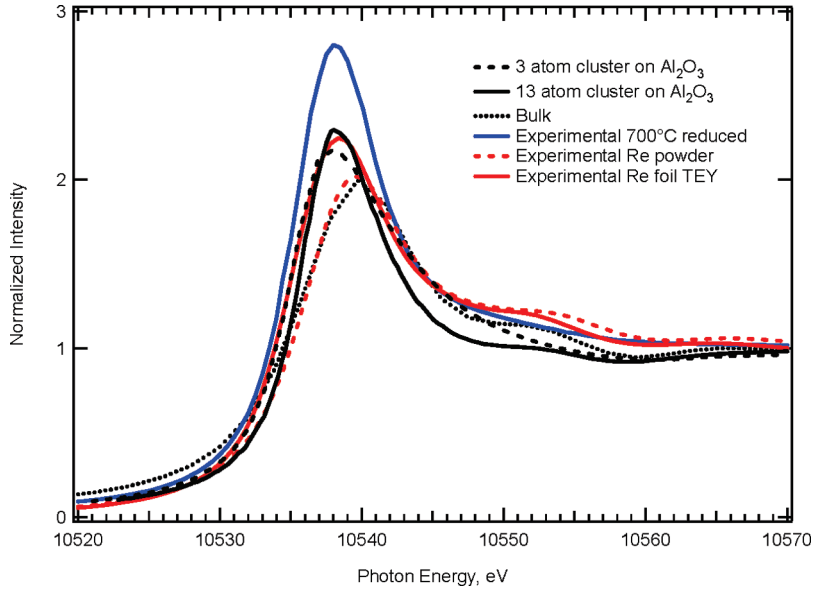

Figure 8. Comparison of the calculated Re L_3-edge XANES of the 3- and 13-atom Re clusters interacting with an alumina surface and the experimental XANES of the 700 °C reduced and Re metal.

after the reduction, in agreement with the STEM data. Interestingly, the Re−Re CN is smaller for the 700 °C reduction spectrum (1.8 ± 0.4) as compared to the 500 °C reduction (2.3 ± 0.4) spectrum. A coordination number of unity would be consistent with the presence of Re dimers after 700 °C reduction, and the CN of 2 after the 500 °C reduction would be indicative of trimers of Re. These EXAFS-derived cluster sizes are not inconsistent with the size of the Re clusters observed in the STEM data. EXAFS measures the average of all of the Re clusters present, whereas the STEM image is dominated by the few larger clusters that are observable. Therefore, one interpretation that brings consistency between STEM and EXAFS is that there are many more highly dispersed Re clusters than STEM-observable clusters.

This initial molecular moiety model indicates both the presence of a Re−O bond at 1.7 Å which is an indication of an oxidic Re species, and thus unreduced, and the presence of a Re−Re bond length of 2.5 Å which is similar to metallic Re. Thus, there is strong evidence for both incomplete reduction of Re and some clustering of reduced Re. Combining this information with the XPS data, the STEM data, and the XANES data (lack of feature at ∼10 553 eV), the conclusion is reached that the majority of the Re must be highly dispersed on the alumina surface. One hypothesis is that the majority of the Re is perhaps monodispersed so that it would not be observed in the STEM (with its limited spatial resolution), resulting in a cationic Re entity that would have dominant Re−O and Re−O−Al scattering signals in EXAFS. To test this hypothesis and to understand how this very dispersed Re would interact with the γ-alumina surface, DFT calculations were performed using monomers of Re. On the basis of these DFT calculations, more complex EXAFS models were

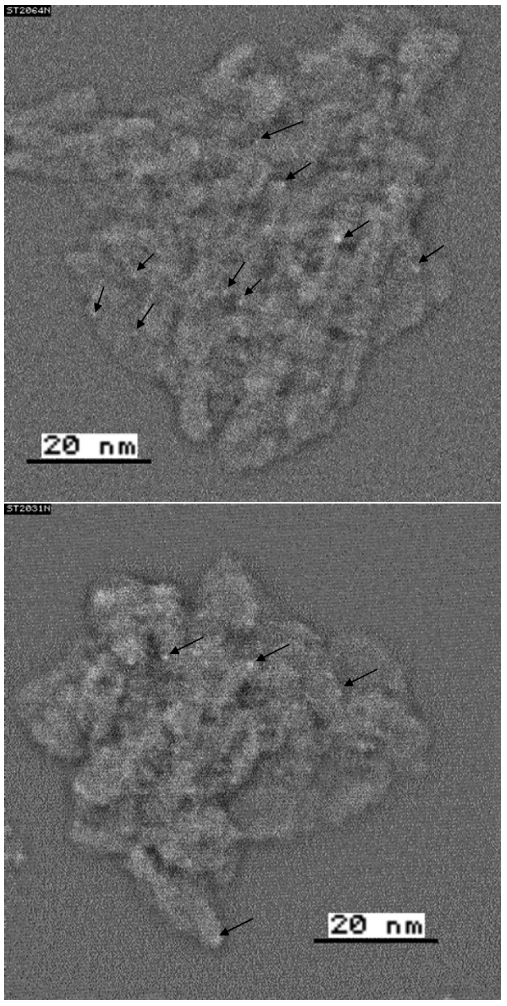

Figure 9. STEM images recorded from the 500 °C reduced sample (upper) and from the 700 °C reduced sample (lower). Arrows indicate the location of metal clusters.

built that allowed actual identification of the dominant adsorption site of the monodispersed Re.

The conformations of the Re atom on the γ-alumina surface that are subsequently used in the resulting more detailed EXAFS models were obtained by means of DFT optimization. The five different adsorption site energy minima, whose structures are shown schematically in Figure 12, were obtained by first mapping the interaction energy of a Re atom located 2.2 Å above the alumina surface, followed by unrestricted relaxation. The starting conformations for these optimizations were chosen at points with the largest interaction energy of the Re atom with the alumina surface: (1) with a doubly coordinated O atom, designated as min1; (2) with a triply coordinated O atom, min2; (3) with a surface octahedral Al atom, min3; (4) with an Al vacancy, min4; and (5) with a doubly coordinated O atom with a horizontal Al−O bond, min5.

With the exception of the triply coordinated O atom site, each of these optimizations finished close to its initial position. At the end of the optimization, the min2 moved from its initially triply coordinated O site to a doubly coordinated one. However, the final structure of min2 is slightly different than the one obtained for min1, which also resides on a doubly coordinated site. In min2, the Re atom is closer to the O atom and slightly to the side.

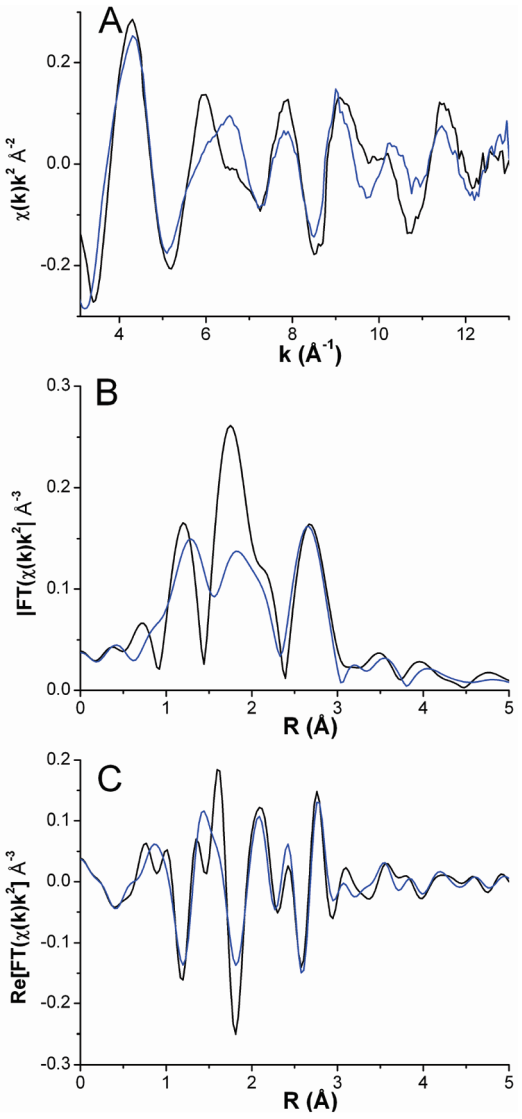

Figure 10. Comparison of Re EXAFS spectra after the 500 °C (black) and 700 °C (blue) reduction. (A) EXAFS $\chi(k)\cdot k^2$. (B) and (C) Magnitude and real part of the Fourier transform.

Table III. EXAFS Modeling Results for the 500 °C and 700 °C Reduction[a]

path description	N_{degen}	R (Å)	σ^2 ($\cdot 10^{-3}$ Å^2)
	500 °C Reduction		
Re−O1	0.9 ± 0.2	1.71 ± 0.02	5
Re−O2	1.0 ± 0.3	1.95 ± 0.02	5
Re−Al1	1.9 ± 0.4	2.86 ± 0.02	9.2
Re−Re	2.3 ± 0.4	2.52 ± 0.01	9.2
	700 °C Reduction		
Re−O1	0.6 ± 0.2	1.73 ± 0.03	5
Re−O2	0.4 ± 0.2	2.06 ± 0.03	5
Re−Al1	1.5 ± 0.4	2.90 ± 0.02	9.2
Re−Re	1.8 ± 0.4	2.52 ± 0.02	9.2

[a] Spectra collected at LN_2 temperature. σ^2 values were held at the values listed.

min1, min2, and min5, in which the Re atom interacts mainly with one or two doubly coordinated O atoms, represent the most common interaction motifs on the γ-Al_2O_3 surface. In these

dx.doi.org/10.1021/jp1105218 |J. Phys. Chem. C 2011, 115, 5740–5755

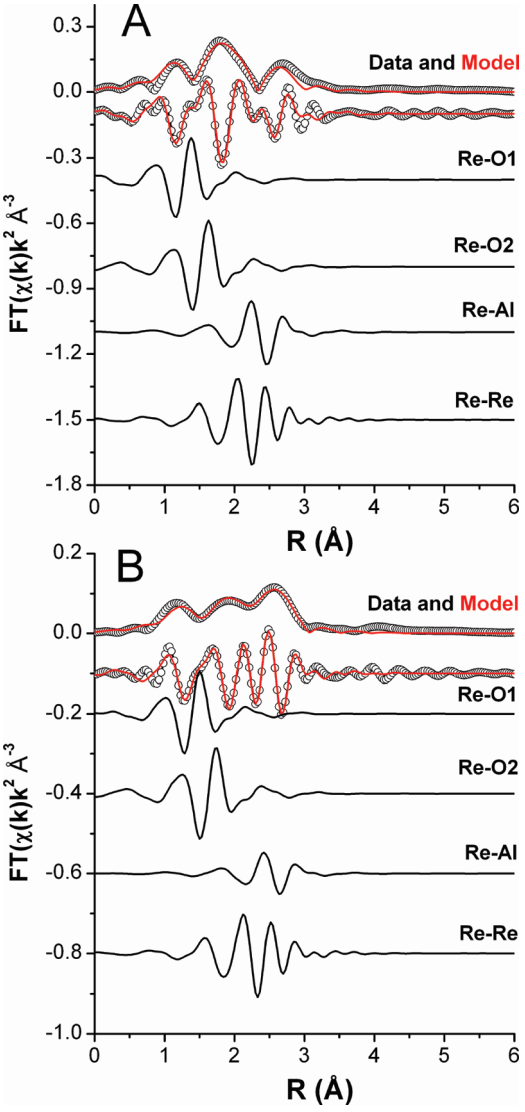

Figure 11. Fourier transform of the Re EXAFS spectra (symbols) from the dry 500 °C reduced (A) and the dry 700 °C reduced (B) and the molecular moiety model (line). In each figure the magnitude is offset from the real part of the Fourier transform. The real part of each component in the model is also shown.

minima, Re−O bonds represent the dominant anchors of the Re atom to the surface. The dominance of the Re−O interactions can also be seen in the case of min3. For this conformation, the initial Re−Al distance is increased in favor of a reduction of the bond distance between the Re and a neighboring O atom. Thus, the Al atoms tend not to be associated with stable interaction sites on the surface. Nevertheless, as seen from the Re−Al bond distances (Supporting Information, Table SVI and corresponding Figure S11), the Re−Al interactions are not negligible. min4 is of special interest since it corresponds to the interaction with an Al vacancy. In this conformation, the Re atom becomes embedded on the surface, closely occupying the location of the vacant Al atom. Moreover, the Re−O bond distances are slightly shorter than for the other minima, probably due to the dangling bonds on the O atoms.

The final EXAFS model builds on the prior molecular moiety model by combining it with the information from the DFT calculations for a monatomic Re species on the alumina surface. This EXAFS model is built using a combination of the model used to describe oxidic Re (as the previously determined ReO_4 species) on alumina weighted by a fraction (designated as $f_{ox}7$ and $f_{ox}5$ for the fraction of oxidic Re after 700 and 500 °C reduction, respectively), Re at the different locations on alumina as determined by DFT calculations (min1−min5), and metallic Re clusters. For the part of the model based on the Re adatoms on the alumina surface, the path lengths for each path in the model were allowed to vary as related to the position of Re on the surface so that only the *X*, *Y*, and *Z* positions of the Re atom at the surface were allowed to change. (The mathematical expressions are not shown.) The reduced χ^2 values scaled to the best model for min2 are: 4, 1, 16, 6, and 23 for min1, min2, min3, min4, and min5, respectively. Only min2 was able to accurately reproduce the measured spectra, as the next best model based on min1 was 4 times less accurate. The resulting EXAFS model based on min2 is significantly better at describing the measured data than the previously described molecular moiety model. The reduced χ^2 value is 10 times greater for the molecular moiety model as compared to the model based on min2 indicating that the details of the measured spectra are more accurately accounted for with the model based on min2. The reduced χ^2 comparison takes into account the different number of variables in these two models. Indeed the molecular moiety model for both data sets includes 18 parameters while the DFT-based model includes 17 parameters. The details of the min2 model are given in Table IV. Several of the DFT-based model parameters (10) are listed in bold type in Table IV. The other seven are the *X*, *Y*, and *Z* position for each data set (6) and one energy shift parameter, which are not shown in the table.

The best fit model based on min2 and the experimental EXAFS data after the 700 and 500 °C reduction temperatures are shown in Figure 13. Figures S12 and S13 (Supporting Information) show the magnitude of the FT of the EXAFS for the molecular moiety model and the best fit model, respectively, for both the 500 and 700 °C reduced catalysts. The best fit values and parametrizations for the EXAFS model based on min2 are listed in Table IV. Values for path lengths belonging to min2 were determined from the (*X*, *Y*, Z) position of Re on the alumina surface. The position of Re on the alumina surface is slightly different for the two reduction temperatures with offset values of (−0.32 ± 0.01 Å, −0.11 ± 0.01 Å, −0.10 ± 0.01 Å) at 500 °C and (−0.18 ± 0.03 Å, −0.11 ± 0.03 Å, −0.01 ± 0.01 Å) at 700 °C from the min2 position. At 500 °C reduction the Re atom is slightly closer to the γ-alumina surface than it is after the 700 °C reduction, as indicated by the larger negative *Z* value. The oxidic percentages are 11 ± 3% ($f_{ox}7$) and 26 ± 2% ($f_{ox}5$) for 700 and 500 °C, respectively. The value for S_0^2 was held at 0.83 as previously determined (see Supporting Information). The energy shift parameter is 5.3 ± 0.9 eV.

The Re−Re CN, adjusted for the amount of oxidic Re, is 2.0 ± 0.4 and 3.4 ± 0.8 for the 700 and 500 °C spectra, respectively. These values are similar considering the uncertainties, but the 500 °C values lean toward a larger size indicating that on average the clusters are somewhat less dispersed at the lower reduction temperature.

The values of oxidic Re remaining in the 500 and 700 °C reduced samples as determined from the final EXAFS model, 26 ± 2% and 11 ± 3%, respectively (determined by the CN listed in Table IV for percentage of 4-fold oxidic Re given in Table I for the oxidized form of the catalyst), are in good agreement with those calculated from the corresponding TPR hydrogen

dx.doi.org/10.1021/jp1105218 |*J. Phys. Chem. C* 2011, 115, 5740–5755

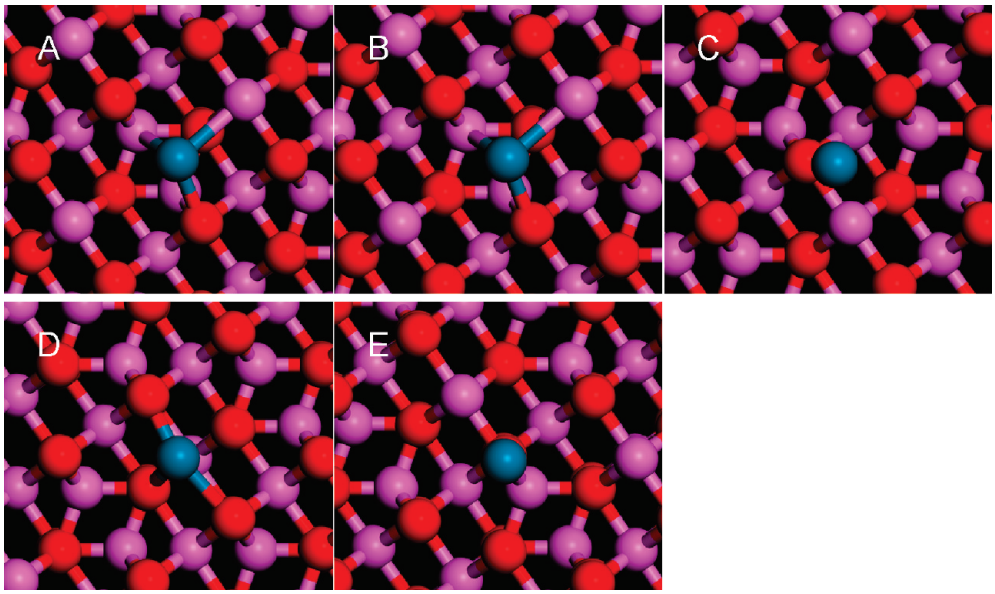

Figure 12. Schematic of the position of the Re atom on the alumina surface. Red, purple, and blue spheres represent O, Al, and Re atoms, respectively. (A) mMin1, (B) min2, (C) min3, (D) min4, and (E) min5.

Table IV. Best-Fit Values and Parameterization for the 700 °C and 500 °C Spectra Based on a Combination of min2, Oxidic 4-Fold Re, and Metallic Re Clusters[a]

path description	data	N_{degen}		R (Å)	σ^2 ($\cdot 10^{-3}$ Å^2)	
			min2			
Re−O1	700	$1\cdot(1-\boldsymbol{f_{ox}}7)$	0.89 ± 0.03	1.91 ± 0.03	$\boldsymbol{\sigma^2}$**O1_7**	17 ± 3
	500	$1\cdot(1-\boldsymbol{f_{ox}}5)$	0.74 ± 0.02	1.95 ± 0.01	$\boldsymbol{\sigma^2}$**O1_5**	1.1 ± 0.4
Re−O2	700	$1\cdot(1-f_{ox}7)$	0.89 ± 0.03	2.41 ± 0.01	$\boldsymbol{\sigma^2}$**O2**	6 ± 1
	500	$1\cdot(1-f_{ox}5)$	0.74 ± 0.02	2.40 ± 0.01		
Re−O3	700	$1\cdot(1-f_{ox}7)$	0.89 ± 0.03	2.35 ± 0.03	σ^2O2	6 ± 1
	500	$1\cdot(1-f_{ox}5)$	0.74 ± 0.02	2.23 ± 0.01		
Re−Al1	700	$1\cdot(1-f_{ox}7)$	0.89 ± 0.03	2.67 ± 0.01	$\boldsymbol{\sigma^2}$**Al1**	7 ± 1
	500	$1\cdot(1-f_{ox}5)$	0.74 ± 0.02	2.75 ± 0.01		
Re−Al2	700	$1\cdot(1-f_{ox}7)$	0.89 ± 0.03	2.43 ± 0.02	σ^2Al1	7 ± 1
	500	$1\cdot(1-f_{ox}5)$	0.74 ± 0.02	2.30 ± 0.01		
Re−Al3	700	$1\cdot(1-f_{ox}7)$	0.89 ± 0.03	2.95 ± 0.02	$\boldsymbol{\sigma^2}$**Al2**	15 ± 4
	500	$1\cdot(1-f_{ox}5)$	0.74 ± 0.02	2.99 ± 0.01		
			4-Fold Oxidic Re			
Re−O1b	700	$3.53^b\cdot f_{ox}7$	0.40 ± 0.06	1.73^b	σ^2O2	6 ± 1
	500	$3.53^b\cdot f_{ox}5$	0.92 ± 0.06	1.73^b		
Re−O2b	700	$0.47^b\cdot f_{ox}7$	0.04 ± 0.01	2.08^b	σ^2O2	6 ± 1
	500	$0.47^b\cdot f_{ox}5$	0.12 ± 0.01	2.08^b		
Re−O1a−Re−O1a	700	$3.53^b\cdot f_{ox}7$	0.40 ± 0.06	3.45^b	$4\cdot\sigma^2$O2	23 ± 3
	500	$3.53^b\cdot f_{ox}5$	0.92 ± 0.06	3.45^b		
			Metallic Re Clusters			
Re−Re	700	$\mathrm{ReCN7}\cdot(1-f_{ox}7)$	2.0 ± 0.4	2.87 ± 0.01	$\boldsymbol{\sigma^2}$**Re**	11 ± 1
	500	$\mathrm{ReCN5}\cdot(1-f_{ox}5)$	3.4 ± 0.8	2.84 ± 0.01		

[a] Parameters in bold are 10 of the 17 parameters determined in the fit. [b] Values held at those found for oxidic Re on alumina.

consumption data, 31.5 and 16%. This agreement between two different methods adds confidence to the conclusion of the fraction of unreduced rhenium.

The overall conclusion is that there are three different rhenium species present on the alumina in the reduced catalyst, and it is the fraction of each that changes with reduction temperature. There is a fraction of unreduced, oxidic Re(VII) present as the trioxo(oxo-aluminate) Re(VII) species, a small number of highly dispersed Re clusters with a maximum size range 5−15 Å, and atomically dispersed Re atoms interacting strongly with the alumina.

4. Wet Hydrogen Reduction. The form of the rhenium in the reduced catalyst is quite different if the reduction is conducted in

dx.doi.org/10.1021/jp1105218 |J. Phys. Chem. C 2011, 115, 5740–5755

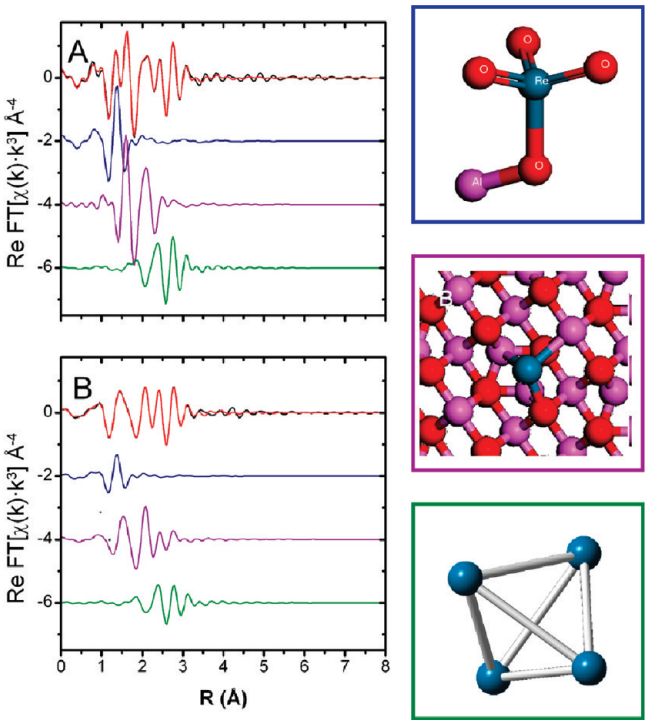

Figure 13. Real part of the Fourier transform of 500 °C (A) and 700 °C (B) EXAFS data (black) and model (red). The components in the model for the oxidic Re (blue), Re atoms on the alumina surface at min2 (purple), and Re clusters (green) are shown offset beneath the data and model. The insets show a representation of these different Re species. From top to bottom they are: oxidic Re, min2, and Re clusters. The blue, red, and purple spheres represent Re, O, and Al atoms.

the presence of moisture. We have previously briefly reported the Re EXAFS data that are obtained after the catalyst is reduced in such a manner.[18] In this experiment the same 0.7 wt % Re catalyst was reduced using a ramp rate of 4 °C/min to 500 °C in a flow of 3.1 mol % H_2O in the hydrogen. Analysis of the Re EXAFS data is consistent with the Re being present as large oblate-shaped clusters with an average diameter in the range of 24−30 Å. Also, using a novel multicompartment ionization chamber detector, we have recently shown that there is growth of the average Re cluster size as a function of bed depth during the reduction.[42] This growth is due to increased moisture levels axially down the bed.

Figure S14 (Supporting Information) shows a comparison of the XAFS following reduction to 500 °C in dry hydrogen, hydrogen containing 1 mol % H_2O, and 3 mol % H_2O. These data are not analyzed further, but there are trends in the EXAFS with increasing moisture: the white line becomes smaller, the intensity of the feature at ∼10 553 eV increases, and the amplitude of the EXAFS becomes larger with increasing moisture. All of these observations are consistent with growth of the rhenium cluster size with increasing moisture levels during the reduction.

5. Air Exposure of Reduced Catalyst. The need for in situ characterization of the reduced catalyst is illustrated by the XAFS data shown in Figure S15 (Supporting Information). The figure shows the XANES and $\chi(k)\cdot k^2$ EXAFS data of an in situ dried catalyst, the same catalyst after a 500 °C reduction, and the same catalyst that had been air exposed to ambient laboratory conditions for two days after the reduction prior to collecting the XAFS data. The similarity of the XAFS data of the fresh oxidized and air exposed reduced catalyst suggests that the reduced Re was readily reoxidized with the exposure to ambient conditions.

DISCUSSION

1. Oxidized Catalyst. All of the characterization data presented indicate that the oxidation state of the rhenium in the dehydrated calcined oxidized catalyst is +7. The EXAFS modeling then shows that this oxidic Re species is present as a trioxo(oxoaluminate) Re(VII) species bound to the alumina surface. Specifically, both the binding energy of the Re $4f_{7/2}$ in the XPS, the absorption edge position, and white line intensity in the XANES data are in agreement regarding the average oxidation state. The EXAFS data are consistent with the rhenium being present as a tetrahedral species, with three short Re−O bonds at 1.73 Å (a Re═O double bond) and one long Re−O bond at 2.08 Å (a Re−O single bond). Due to the presence of a well-defined scattering path due to an Al atom at 3.03 Å (assumed to be from a Re−O−Al bond), it is surmised that the trioxo(oxoaluminate) Re(VII) species is tethered to the alumina surface via the long Re−O bond as a unidentate species. There is no indication of a Re−Re scattering path originating from a Re−O−Re species. Thus, it is concluded that rhenium oxide species are highly dispersed on the alumina surface, and there are no dimers or polymeric oxidic species present. This conclusion is in agreement with most prior work on this catalyst system. Vuurman et al.[43] using in situ laser Raman spectroscopy identified vibrational bands at 1004, 890, and 340 cm^{-1} under dehydrated conditions for an equivalent wt % of rhenium used in this study. These vibrational modes were assigned to the symmetric stretching, antisymmetric stretching, and bending modes, respectively, of a unidentate complex of a "perrhenate ion" coordinated to the alumina surface via one oxygen atom and three terminal Re═O bonds in a C_{3v} configuration. They concluded that the rhenium oxide species is isolated on the surface as they were not able to detect any evidence of vibrational modes that could be assigned to Re−O−Re linkages. This catalyst system was re-examined by Raman spectroscopy by Mitra et al.,[12] and they reached the same conclusions: the rhenium oxide is present as an isolated species and four-coordinated with C_{3v} symmetry with three terminal Re═O bonds.

Comparing our XAFS results to prior EXAFS studies, the only relevant studies that we have identified are those of Ellison et al.[13] and Rønning et al.[16] In the former study, following calcination in air at 525 °C, for a 15 wt % Re catalyst they interpreted their data using four O atoms at 1.73 Å, but for the 10 wt % Re catalyst they needed to slightly distort the coordination environment to two O atoms at 1.71 Å and two atoms at 1.74 Å. In either case they found no evidence for Re−Re interactions. In the latter study, for a 2 wt % Re/Al_2O_3 catalyst calcined at 400 °C, Rønning et al. were able to model their EXAFS data using four O atoms at 1.74 Å and concluded that the Re was present in the +7 oxidation state. Our EXAFS data are conceptually in agreement with these prior studies; the oxidic rhenium species is present in an isolated four-coordinate complex. We have, however, shown that under our experimental conditions the data are statistically better modeled using two different Re−O bond lengths and a Re−O−Al bond.

It has previously been shown using FTIR that changes in the intensities of the hydroxyl bands upon increasing loading of rhenium point to the selective consumption of alumina OH groups by the deposited rhenium.[44,45] During the impregnation the ReO_4^- ions interact predominantly with the basic alumina

hydroxyls. The result is that at a low loading of Re, as used here, the Re is highly dispersed on the alumina surface as the dispersion is dictated by the initial concentration of the most basic OH groups on the alumina surface. The resulting interaction between the perrhenate species and the alumina is strong.

While we have not studied the hydrated oxidic species in any detail due to the uncontrolled level of hydration in our experiments, it is clear that there are subtle changes in the Re L_3-edge XANES between hydrated and dehydrated oxidic species (Supporting Information, Figure S6). It is assumed that these changes are associated with the change of the Re species on the surface from a hydrated or partially hydrated $[ReO_4]^-_{(aq)}$-type species[43] to one of a well-defined trioxo(oxoaluminate) Re complex bound to the alumina surface, as discussed above. There is also a shift in the symmetric Re−O stretching mode between hydrated (ambient, at 982 cm^{-1} for low loadings) and in situ dehydrated (1004 cm^{-1}) Re/Al_2O_3 catalysts as measured by laser Raman spectroscopy.[12,43] Under ambient conditions the Raman is interpreted as the rhenium being present as the perrhenate, ReO_4, ion, as under aqueous conditions. Under dehydrated conditions a unidentate complex is formed where the perrhenate ion coordinates via one oxygen to the alumina surface, leaving three terminal Re═O bonds, resulting in a trioxo(oxoaluminate) Re(VII) species.

2. Reduced Catalyst. In contrast to the speciation of the rhenium in the oxidized catalyst, where the EXAFS data are fully consistent with only a single rhenium species being present, the situation is more complex following reduction. This complexity arises due to the strongly oxophilic nature of the rhenium and the resulting strong interaction with the alumina surface, especially at the relatively low wt % metal loading used here. This manifests itself both in the difficulty in fully reducing the rhenium to the metallic species and in the formation of isolated rhenium atoms on the alumina surface after reduction, resulting in the presence of multiple rhenium species on the alumina—even after reduction at relatively high temperature (700 °C for 30 min). This complexity has been noted previously by Fung et al.,[15] who concluded (based on their EXAFS modeling) that after reduction at 500 °C there was incomplete reduction and that the rhenium was present as a mixture of reduced and oxidic species, and by Rønning et al.[16] who also, based on their EXAFS data, concluded that there was both reduced and unreduced rhenium present following the 6 h reduction at 450 °C. The oxidic rhenium(VII) was identified by the short Re−O distance of 1.74 Å.

Our EXAFS data (taken together with the TPR, XPS, and STEM data) are consistent with a fraction of the rhenium being present as unreduced oxidic Re(VII) species, nanoclusters of Re (larger clusters observable by STEM, smaller ones not detectable), and the majority present as highly dispersed isolated Re atoms on the alumina surface. Moreover, by use of DFT calculations, the preferred location of these isolated Re atoms on the γ-Al_2O_3 surface has been determined, resulting in a detailed characterization of the species present in the reduced Re/ γ-Al_2O_3 catalyst.

Nanoclusters of Re. Nanoclusters of Re are clearly identified using the STEM, where instances of 5−8 Å diameter Re clusters are observed after 500 °C reduction and 5−15 Å diameter Re clusters after 700 °C reduction. The frequency at which these clusters are observed is low, and too few are observed given the metal loading from comparable studies of similar metal loading of, e.g., Pt on alumina on the same instrument, indicating that the majority of the rhenium is not observed in the STEM. The STEM is capable of imaging Group VIII metal clusters of 5 Å diameter, so this gives an upper size estimate of the clusters. The EXAFS modeling is consistent with a Re−Re coordination number of 2 ± 0.4 after 700 °C reduction and 3.4 ± 0.8 after 500 °C reduction. An 8 Å diameter Re cluster based on a spherical cluster model would have a first shell Re−Re CN of 3.16 (containing 19 atoms), and based on a hemispherical Re cluster it would have a first shell Re−Re CN of 2.31 (containing 13 atoms), respectively. Both of these are consistent with the CNs obtained from the EXAFS fitting. However, as pointed out by Fung et al.[15] the CN is the average over all of the Re in the sample, and thus the measured CN is modified by the fraction of Re that is in the metallic state. Unfortunately, as in the case of Fung et al., we also do not know this fraction.

Unreduced Re. The fact that a short Re−O bond of 1.73 Å is determined in the EXAFS fitting implies that this rhenium remains as Re(VII). If the reasonable assumption is made that the local coordination around this Re(VII) center is the same as that in the original oxidized catalyst, then it is relatively straightforward to extract the fraction of unreduced Re following the reduction at the two temperatures (using the determined coordination number). These values are 26 ± 2% and 11 ± 3%, after 500 and 700 °C reduction, respectively. Given the assumptions that are involved in the analysis, it is pleasing to find that these values are in good agreement to those calculated from the corresponding respective TPR hydrogen consumption data, 31.5 and 16% for 500 and 700 °C reduction, respectively, and provide confidence in the estimation of the amount of unreduced rhenium. The fundamental reason why a fraction of the rhenium is so difficult to reduce, while the majority readily reduces between 300 and 400 °C, is not known and will be the focus of future studies. The TPR data in Figure S7 (Supporting Information) show that at low Re loading (0.15 wt %) all of the Re is difficult to reduce, and it is only at a loading >0.15 wt %, where this difficult-to-reduce Re saturates, that the low-temperature reduction peak becomes evident. It is surmised that this results from a combination of the nature of the strong interaction between the initial perrhenate-like species and the hydroxyl groups on the alumina surface, coupled with the oxophilic nature of the Re. The difficult to reduce oxidic Re is that fraction that interacts most strongly with the alumina. Thus, it is hypothesized that the amount of this fraction of difficult-to-reduce rhenium will vary depending on the treatment and type of alumina support that is used (e.g., by using θ-alumina vs γ-alumina as the support).

Isolated Re Atoms. The experimental EXAFS data could not be satisfactorily fit assuming only the presence of oxidic Re and Re nanoclusters. It was thus assumed that some of the Re must be present in a highly dispersed phase. Given that the rhenium in the original calcined catalyst is present as an isolated species, it was surmised that these isolated species existed also in the reduced catalyst, i.e., as single Re atoms strongly interacting with the alumina surface. (The presence of single metal atoms on a catalyst support has recently been directly observed using aberration-corrected STEM.[46]) DFT calculations were performed for Re adatoms on the alumina surface and clearly identified specific sites on the alumina surface with stronger interaction for the location of the Re adatom. Using these energy-minimized structures, the resulting EXAFS models were built that allowed actual identification of the dominant adsorption site of the monodispersed Re. It is believed that this is the first time such calculations have been coupled with experimental EXAFS data for adatoms on a catalyst support. The combined EXAFS model based on the DFT-minimized location of isolated Re atoms, unreduced trioxo(oxoaluminate) Re(VII) groups, and nanoclusters of rhenium (Figure 13) results in a statistically significantly better agreement with

the experimental data than a simple molecular moiety model (Figure 11).

Reduction. There is an offset in the maximum rate of reduction between the TPR data, with a maximum rate at 375 °C (Figure 2), and the TPR-XANES data, with a maximum rate at 300 °C (Figure 3). This offset is a result of the hydrogen partial pressure dependence of the reduction and has been noted and discussed previously.[47,48] We have not studied this effect in detail here. However, we have determined that the maximum rate of reduction is also a function of the ramp rate (data not shown) that is used during the reduction. It is suggested that some of the discrepancy in the literature over the temperature of the reduction and the amount of reducible rhenium is a result of the complex interplay between the type and treatment of the alumina used as the support which governs the distribution of strongly and more weakly bound rhenium, the hydrogen partial pressure used during the reduction, whether the catalyst is predried, and the ramp rate used in the experiment. All of these need to be controlled when using TPR methods to compare different alumina-supported rhenium catalysts.

XANES. As we and others have shown, the Re L_3-edge white line of a reduced alumina-supported Re catalyst is enhanced over that from metallic rhenium. For example, Fung et al. showed that the intensity of the white line is the same from a sample shown to contain only trirhenium clusters as that prepared from impregnation with ammonium perrhenate and is the same as that as ReO_2.[15] They concluded that the rhenium is cationic, with an average oxidation state of 4. This was the case both for the Re trimer and for the sample with significantly larger clusters prepared from the perrhenate. Our experimental data shown in Figure 4 are conceptually in agreement with this work: the edge position corresponds to that of Re(0), but the intensity is similar to that of Re(IV) oxide. It has been shown from the EXAFS modeling, combined with the other characterization data, that for both the 500 and 700 °C reduced samples the Re is present as a combination of trioxo(oxoaluminate) Re(VII), isolated Re atoms interacting strongly with the alumina surface, and Re nanoclusters with a range of sizes. The relative fraction of these species changes with reduction temperature. However, the XANES data are relatively insensitive to these changes—there is only a subtle difference between the XANES of the 500 and 700 °C reduced samples. The calculated Re L_3-edge XANES of the small Re clusters on the alumina surface sheds some understanding on the origin of the enhanced white line in the reduced sample compared to that expected for metallic Re. The data in Figure 7 show an enhanced white line of 3- and 13-atom Re clusters interacting with an alumina surface, but the intensity is markedly suppressed from that of the naked clusters (Figure 5). This intensity difference can be related to a difference in the density of states of the supported clusters compared to the naked clusters. The LDOS of the supported clusters is much broader, reflecting a reduction in symmetry. The absorption edge position of these calculated clusters matches well the experimental data. Using the FEFF XANES calculations of the small supported Re clusters as a guide, it is surmised that the XANES of the isolated Re atoms dispersed on the alumina would also have a strongly enhanced white line, and likely larger than that of the 3-atom cluster. Thus, we believe that the enhanced white line is a manifestation of the highly dispersed nature of the Re. It is still not understood why the XANES is not sensitive to the presence of the trioxo(oxoaluminate) Re(VII) component in the unreduced catalyst.

One interesting result from the theoretical XANES calculations is the potential use of the resonance at ~10 553 eV as a rough guide to Re cluster size. This feature only becomes pronounced in the XANES when there are >20 atoms in the Re cluster. Comparing the calculated spectra to those from numerous reduced catalysts supports the idea that the size of this feature can be used as a qualitative measure of the size of the cluster.

Wet Hydrogen Reduction. Reduction of the rhenium in the presence of moisture affects the average Re cluster size obtained. There is growth in the average cluster size with increased moisture. These data indicate that the moisture level needs to be controlled during the reduction if the purpose is to obtain highly dispersed Re. It is not known from these studies what the mobile Re species is in the presence of moisture, but it is likely related to the degree of hydroxylation of the alumina. The mobility of Re on γ-alumina has been observed and discussed previously, but no consensus has been reached as to the detailed mechanism and is beyond the scope of this study.[49−51] It is thought that water vapor increases the mobility of metal atoms or metal complexes on the support due to adsorbed water or hydroxyl groups.[52]

SUMMARY

In a calcined dried alumina-supported Re catalyst, prepared from ammonium perrhenate, the Re species is present as an isolated trioxo(oxoaluminate) Re(VII) species. This species has three Re−O bonds with a bond length of 1.73 ± 0.01 Å and one Re−O bond with a bond length of 2.08 ± 0.01 Å. The species is tethered to the alumina surface, and the resulting Re−O−Al scattering path is clearly identifiable in EXAFS.

The temperature at which the Re undergoes reduction is a function of the hydrogen partial pressure and ramp rate, but the maximum rate of reduction occurs in the range 300−400 °C.

Following reduction at 500 or 700 °C in dry hydrogen, the Re is present as a mixture of species: unreduced Re(VII) species, Re nanoclusters, and isolated Re atoms. The fraction of unreduced Re varies from around 30% after the 500 °C reduction to approximately 16% after the 700 °C reduction. The distribution of the reduced Re species between the nanoclusters and single adatoms cannot be calculated. However, by taking into account all of the characterization data it is surmised that the majority species is an isolated Re adatom bound to the alumina support. DFT calculations were used to identify the most likely adsorption site for these Re adatoms on the [110] surface of γ-Al_2O_3. The final EXAFS model taking into account these three species is in very good agreement with the experimental data.

The Re L_3-edge XANES of the reduced catalyst has an edge position similar to that of metallic Re but an intensity similar to that of Re(IV). FEFF8 XANES calculations of free and alumina-supported Re nanoclusters provide some interpretation of this observation.

The presence of moisture present during the reduction strongly affects the mobility of the Re on the alumina leading to agglomeration. Subsequent air exposure of a reduced catalyst readily reoxidizes the reduced Re.

ASSOCIATED CONTENT

Supporting Information. Additional experimental details. This material is available free of charge via the Internet at http://pubs.acs.org.

AUTHOR INFORMATION

Corresponding Author

*E-mail: simon.bare@uop.com.

Present Addresses

⊥Bruker AXS GmbH, Beijing, China.

ACKNOWLEDGMENT

Steve Bradley, Sue Tonnesen, and Norma Kahn, all at UOP, are thanked for the STEM data, the TPR data, and the XPS data, respectively. Use of the Advanced Photon Source, an Office of Science User Facility operated for the U.S. Department of Energy (DOE) Office of Science by Argonne National Laboratory, was supported by the U.S. DOE under Contract No. DE-AC02-06CH1135. Use of the National Synchrotron Light Source, Brookhaven National Laboratory, was supported by the U.S. Department of Energy, Office of Science, Office of Basic Energy Sciences, under Contract No. DE-AC02-98CH10886. This work is also supported in part by the U.S. Department of Energy, Office of Basic Energy Sciences, grant DE-FG02-97ER45623 (JJR and FV).

REFERENCES

(1) Mol, J. C. *Catal. Today* **1999**, *51*, 289.
(2) Yuan, Y. Z.; Shido, T.; Iwasawa, Y. *Chem. Commun.* **2000**, 1421.
(3) Wang, C.-B.; Cai, Y.; Wachs, I. E. *Langmuir* **1999**, *15*, 1223.
(4) Escalona, N.; Ojeda, J.; Cid, R.; Alves, G.; Agudo, A. L.; Fierro, J. L. G.; Llambias, F. J. G. *Appl. Catal., A* **2002**, *234*, 45.
(5) Sinfelt, J. H. In *Handbook of Heterogeneous Catalysis*; Ertl, G., Knözinger, H., Weitkamp, J., Eds.; VCH: Weinheim, Germany, 1997; Vol. 4, p 1939.
(6) Antos, G. J.; Aitani, A. M. *Catalytic Naphtha Reforming*; 2nd ed., Revised and Expanded; Marcel Dekker, Inc.: New York, 2004.
(7) Webb, A. N. *J. Catal.* **1975**, *39*, 485.
(8) Johnson, M. F. L.; LeRoy, V. M. *J. Catal.* **1974**, *35*, 434.
(9) McNicol, B. D. *J. Catal.* **1977**, *46*, 438.
(10) Wang, L.; Hall, W. K. *J. Catal.* **1983**, *82*, 177.
(11) Arnoldy, P.; van Oers, E. M.; Bruinsma, O. S. L.; De Beer, V. H. J.; Moulijn, J. A. *J. Catal.* **1985**, *93*, 231.
(12) Mitra, B.; Gao, X. T.; Wachs, I. E.; Hirt, A. M.; Deo, G. *Phys. Chem. Chem. Phys.* **2001**, *3*, 1144.
(13) Ellison, A.; Diakun, G.; Worthington, P. *J. Mol. Catal.* **1988**, *46*, 131.
(14) Hardcastle, F. D.; Wachs, I. E.; Horsely, J. A.; Via, G. H. *J. Mol. Catal.* **1988**, *46*, 15.
(15) Fung, A. S.; Tooley, P. A.; Kelley, M. J.; Koningsberger, D. C.; Gates, B. C. *J. Phys. Chem.* **1991**, *95*, 225.
(16) Ronning, M.; Nicholson, D. G.; Holmen, A. *Catal. Lett.* **2001**, *72*, 141.
(17) Lobo-Lapidus, R. J.; Gates, B. C. *J. Catal.* **2009**, *268*, 89.
(18) Yang, N.; Mickelson, G. E.; Greenlay, N.; Kelly, S. D.; Vila, F. D.; Kas, J.; Rehr, J. J.; Bare, S. R. *AIP Conf. Proc.* **2007**, *882*, 591.
(19) Okal, J. *Pol. J. Chem.* **2002**, *76*, 1505.
(20) Okal, J. *Appl. Catal., A* **2005**, *287*, 214.
(21) Okal, J.; Baran, J. *J. Catal.* **2001**, *203*, 466.
(22) Okal, J.; Kepinski, L.; Krajczyk, L.; Drozd, M. *J. Catal.* **1999**, *188*, 140.
(23) Okal, J.; Kepinski, L.; Krajczyk, L.; Tylus, W. *J. Catal.* **2003**, *219*, 362.
(24) Okal, J.; Tylus, W.; Kepinski, L. *J. Catal.* **2004**, *225*, 498.
(25) Okal, J.; Kepinski, L. In *Focus on Catalysis Research*; Bevy, L. P., Ed.; Nova Science Publishers, Inc.: Hauppauge, N. Y., 2006; p 21.
(26) Shpiro, E. S.; Avaev, V. I.; Antoshin, G. V.; Ryashentseva, M. A.; Minachev, K. M. *J. Catal.* **1978**, *55*, 402.
(27) Yide, X.; Xinguang, W.; Yingzhen, S.; Yihua, Z.; Xiexian, G. *J. Mol. Catal.* **1986**, *36*, 79.
(28) Bare, S. R.; Mickelson, G. E.; Modica, F. S.; Ringwelski, A. Z.; Yang, N. *Rev. Sci. Instrum.* **2006**, *77*, 023105/1.
(29) Perdew, J. P.; Burke, K.; Ernzerhof, M. *Phys. Rev. Lett.* **1996**, *77*, 3865.
(30) Vanderbilt, D. *Phys. Rev. B* **1990**, *41*, 7892.
(31) Kresse, G.; Furthmüller, J. *Phys. Rev. B* **1996**, *54*, 11169.
(32) Ankudinov, A. L.; Bouldin, C. E.; Rehr, J. J.; Sims, J.; Hung, H. *Phys. Rev. B* **2002**, *65*, 104107.
(33) Ankudinov, A. L.; Rehr, J. J.; Low, J. J.; Bare, S. R. *Top. Catal.* **2002**, *18*, 3.
(34) Hedin, L.; Lundqvist, S. *Solid State Phys.* **1969**, *23*, 1.
(35) Ravel, B.; Newville, M. *J. Synchrotron Radiat.* **2005**, *12*, 537.
(36) Newville, M. *J. Synchrotron Radiat.* **2001**, *8*, 322.
(37) Stern, E. A.; Newville, M.; Ravel, B.; Yacoby, Y.; Haskel, D. *Phys. B-Condens. Matter* **1995**, *208*, 11.
(38) Rehr, J. J.; Albers, R. C. *Rev. Mod. Phys.* **2000**, *72*, 621.
(39) Brillouin, L. *Science and Information Theory*; Academic Press: New York, 1967.
(40) Kelly, S. D.; Bare, S. R.; Greenlay, N.; Azevedo, G.; Balasubramian, M.; Barton, D.; Chattopadhay, S.; Fakra, S.; Johnnessen, B.; Newville, M.; Pena, J.; Pokrovski, G. S.; Proux, O.; Priolkar, K.; Ravel, B.; Webb, S. M. *J. Phys.: Conf. Ser.* **2009**, *190*, 012032.
(41) Ravel, B.; Scorzato, C.; Siddons, D. P.; Kelly, S. D.; Bare, S. R. *J. Synchrotron Radiat.* **2010**, *17*, 380.
(42) Bare, S. R.; Kelly, S. D.; Ravel, B.; Greenlay, N.; King, L.; Mickelson, G. E. *Phys. Chem. Chem. Phys.* **2010**, *12*, 7702.
(43) Vuurman, M. A.; Stufkens, D. J.; Oskam, A.; Wachs, I. E. *J. Mol. Catal.* **1992**, *76*, 263.
(44) Turek, A. M.; Wachs, I. E.; DeCanio, E. *J. Phys. Chem.* **1992**, *96*, 5000.
(45) Sibeijn, M.; Spronk, R.; van Veen, J. A. R.; Mol, J. C. *Catal. Lett.* **1991**, *8*, 201.
(46) Blom, D. A.; Bradley, S. A.; Sinkler, W.; Allard, L. F. *Microsc. Microanal.* **2006**, *12*, 50.
(47) Bare, S. R.; Yang, N.; Kelly, S. D.; Mickelson, G. E.; Modica, F. S. *Catal. Today* **2007**, *126*, 18.
(48) Bolivar, C.; Charcosset, H.; Frety, R.; Primet, M.; Tournayan, L.; Beitzeau, C.; Leclerq, C.; Maurel, R. *J. Catal.* **1975**, *39*, 249.
(49) Ziemecki, S. B.; Jones, G. A.; Michel, J. B. *J. Catal.* **1986**, *99*, 207.
(50) Wagstafff, N.; Prins, R. *J. Catal.* **1979**, *59*, 434.
(51) Isaacs, B. H.; Petersen, E. E. *J. Catal.* **1982**, *77*, 43.
(52) Bartholemew, C. H. *Stud. Surf. Sci. Catal.* **1994**, *88*, 1.